# Influence of Transfer Molding Process on the Reliability of High Mass Epoxy Mold Compound Molded Package

Dong Hu[1], Niek van Haare[1], Albert van Driel[1], Shatavisha Biswas[2], Sten Vollebregt[2], Sebastiaan Kersjes[1]

[1] Besi Netherlands B.V., The Netherlands
[2] Delft University of Technology, The Netherlands

Corresponding author: Dong Hu, dong.hu@besi.com
Speaker: Dong Hu, dong.hu@besi.com

## Abstract

Overmolding power modules consumes more epoxy molding compound (EMC) than molding discrete devices. The increased EMC mass affects the heating of the EMC, which in turn affects flow viscosity. In this study, the effects of the number of EMC pellets and their pretreatment on flow temperature evolution were investigated using an experimental melting test rig. Additionally, dummy plastic leaded chip carrier (PLCC) leadframes were overmolded with (non-)preheated pellets at temperatures of 175 °C and 165 °C. The molded products were subsequently aged at 200 °C for 600 hours. Pellet preheating plays a more essential role than molding temperature in the encapsulation reliability, providing the lowest porosity and thinnest thermal oxide layer over the thermal exposure.

## 1 Introduction

Epoxy molding compounds (EMC) are widely used in encapsulating microelectronic devices to protect chips from external environmental impacts. Transfer molding is a flexible and versatile technology that enables many semiconductor applications, e.g. RF module [1], LED optics [2] and organ-on-chips [3], etc.

Regarding power electronics, the increasing demand for high-power density and efficiency in automotive and industrial applications has driven the growth of the power module market [4, 5]. As a result, there is a trend in encapsulation materials by switching from silicone gel to EMC thanks to the great high-temperature stability. Further, transfer molding with EMC enables mechanically robust power modules with effective cost [6, 7]. However, to facilitate high power density and high integration levels, the volume of products become larger. Compared to discrete device packaging, overmolding power modules consume more EMC. The higher mass hinders temperature increase of the EMC pellets. If not mitigated this risk lower temperatures in the EMC pellets lead to longer filling times due to high viscosity and high risk to entrap air in the molding product.

To address this topic, it is essential to investigate the relationship between transfer process parameters and melting behavior. Moreover, thermal oxide growth during thermal aging significantly affects the thermomechanical performance of the product [8, 9]. Thus, the impact of the transfer process on encapsulation reliability performance is also of interest.

In this study, different numbers of pellets with various pretreatments were subjected to a melting test rig. The flow temperature evolution was measured during a constant pressure-driven transfer process, while finite element method (FEM) simulations were conducted to gain a deeper understanding of the flow trajectory. Furthermore, plastic leaded chip carrier (PLCC) packages were overmolded using (non-) pretreated pellets and subjected to high-temperature storage (HTS) aging at 200 °C for 600 hours. The porosity and thermal oxide growth were monitored throughout the thermal exposure.

## 2 Experimental methods

### 2.1 Preparation of samples

In this study, a commercial grade EMC A is used, which contains 70-90% amorphous silica as fillers. The length of one pellet is 15.7 mm and the diameter is 14 mm. Pellet preheating is performed by an in-house built setup, consisting of a pellet

ISBN: 978-3-8007-6541-6

holder and a hot plate at 70 °C. as experiment a 15-minute preheating time is applied to ensure uniform pellets temperature distribution.

## 2.2 Experimental methods - Pellets melting

Figure 1(a) presents a melting test rig, which is in-house built to mimic the pellets melting stage in the practical transfer process. Pellets are transferred through a hot sleeve by plunger. Pellets melt on the surface of a heat transfer plug. The melted EMC flow goes along the hot runner region, which connects to the atmospheric environment. A type-K thermocouple is placed closing to the end of the runner, probing into the middle of the EMC flow. The temperature of test rig is controlled by PT-100 at 180°C. The plunger is driven by constant 4.0 bar air pressure. The data acquisition is conducted by a DATAQ DI-4108-E data logger with a sampling rate of 1 kHz. The trigger of data acquisition is synchronized with activating plunger movement. The signals of plunger displacement and thermocouple temperature are recorded for 30 seconds.

## 2.3 Experimental methods - Overmolding PLCC packages with a research-oriented recipe

Dummy PLCC leadframes were molded in a BESI Fico MMS-I transfer molding machine. The same EMC A pellets were applied in the molding shots, where two pellets were loaded in one sleeve. A research-oriented PLCC recipe is applied, which can produce a certain level porosity as a reference. The key parameters are listed in Tab. 1. After molding, a 4-hour post mold curing (PMC) was performed in a UFPlus Memmert climate chamber at 150 °C.

| Parameter | Value |
|---|---|
| Molding temperature | 165/175 °C |
| Transfer pressure | 11 MPa |
| Curing time | 180 s |
| Clamping force | 500 kN |
| Cavity vacuum | N/A |
| PMC temperature | 150 °C |
| PMC time | 4 h |

**Table 1** Key process parameters in the research-oriented recipe of molding PLCC packages.

## 2.4 FEM Simulation on air entrapment

FEM simulation of the flow of melted EMC is conducted in Simcenter FLOEFD software. The turbulent flow was predicted by solving the Fravre-averaged Navier-Stokes equations where time-averaged effects of the flow turbulence on the flow parameters are considered.

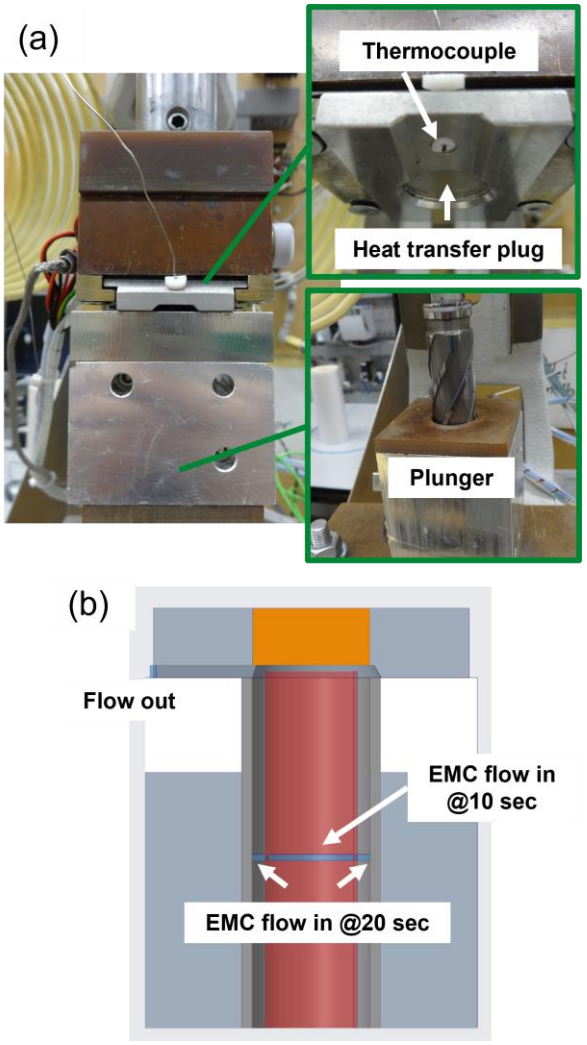


**Fig. 1** The structure of the melting test tig (a) experimental setup (b) FEM geometry.

The geometry displayed in Fig. 1(b) is based on the melting test rig. To simplify the model, the EMC is treated as in liquid phase, flowing in from the bottom and exiting through the runner slit. A sleeve surrounding the EMC was added to simulate the EMC flow melted from the bottom of pellets.

Initially, the fluid domain is filled with air, and the liquid EMC begins to flow after 10 seconds to simulate the plunger movement at a speed of 1 mm/s. The surrounding region starts to receive EMC flow after 20 seconds at the same speed, simulating the melted EMC at the bottom.

The environment is set as 180 °C while the initial temperature of the EMC is 25 °C. Thermophysical properties of the EMC are adopted from [10].

## 2.5 High temperature storage aging test

The overmolded products were subjected to HTS accelerated aging tests in a UFPlus Memmert

 

climate chamber at 200 °C, as per the JESD22-A103D standard [11]. The total aging time was set to 600 hours, with specimens removed every 150 hours for inspection. The voids are characterized by scanning acoustic microscopy (SAM). The thickness of oxide layer is measured by optical microscope from cross sections.

# 3 Results and discussion

## 3.1 Specific heat capacity calibration

Before diving into the analysis of melting performance, the specific heat capacity of the EMC was determined at 160 °C and 200 °C to estimate the average flow temperature in the melting test rig. The calibration was achieved by using solidified EMC outside the runner slit as excessive EMC inserted in Fig. 2.

Six shots were conducted by transferring 3 non-preheated pellets at 180°C and experienced 4-hour 150°C PMC to get fully cured. Subsequently, the EMCs were placed in an oven at 160 °C and 200 °C, respectively, to adsorb sufficient thermal energy. At last, the specific heat capacity of the EMC was calibrated in a calorimeter by measuring the water temperature increase using Eq. (1).

$$Q = c \times m \times \Delta T \quad (1)$$

where $Q$ is heat, $c$ is specific heat capacity of the substance, m is the mass of the substance and $\Delta T$ is the temperature change before and after adsorbing heat.

The calibration results are displayed in Fig. 2. The calculated values at 160 °C and 200 °C are 0.897 and 0.905 J/g·K, respectively. A minor temperature dependency is found. Therefore, by taking the average, the specific heat capacity of the EMC is determined as 0.901 J/g·K. Besides, the density of the EMC was measured as 1.66 g/cm$^3$.

## 3.2 Effect of preheating on the melting performance

Figure 3 illustrates the melting results from 2 and 3 preheated and non-preheated pellets by plotting the evolution of plunger position and temperature. The dashed lines represent the results for non-preheated pellets, while the solid lines correspond to preheated pellets.

In terms of plunger position evolution, the red curve is the reference curve with no pellets loaded. Significant deviation is found between reference curve and the curves with pellets used. The separation point can be understood as the pellets crushing position. The pellets struggle to transition

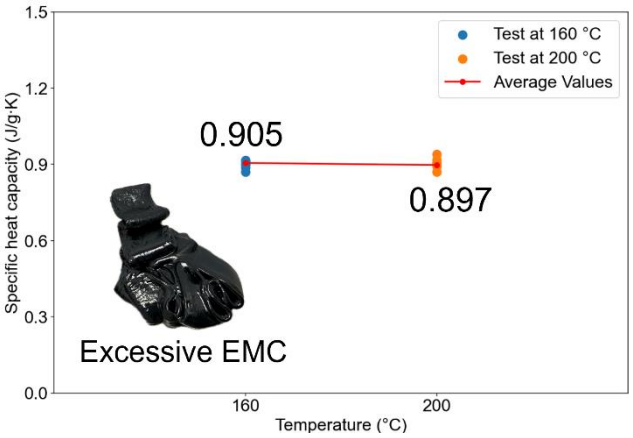


**Fig. 2** Calibration of the specific heat capacity of fully cured EMC.

into a low-viscosity flow upon reaching the heat transfer plug surface due to needed heat transfer, resulting in significant resistance to plunger movement. At the end, the transfer process completes as the plunger position steps into a flat stage. Thus, a shorter transfer time correlates with a higher average velocity.

This result reveals that transfer time is highly dependent on the pellets pretreatment, regardless of the number of pellets used. For non-preheated pellets, the transfer times are 13.53 seconds for 2 pellets and 14.08 seconds for 3 pellets. In contrast, for preheated pellets, the transfer times decrease to 12.85 and 13.15 seconds, respectively.

A more pronounced difference is observed in the temperature evolution. The thermocouple is

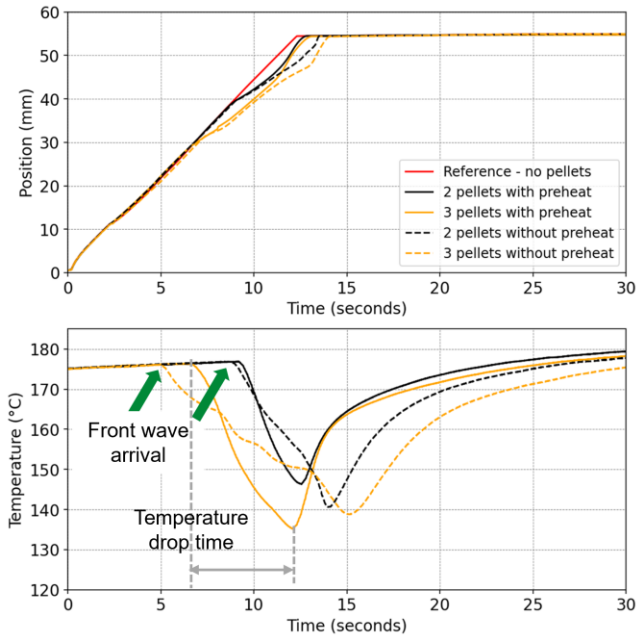


**Fig. 3** Melting performance of 2 and 3 (non-) preheated pellets. (Top) Plunger position evolution; (Bottom) Temperature evolution during the transfer process.

positioned near the end of the runner region. Initially, the runner temperature continuously increases after the test rig closes, as the front wave has not yet reached the thermocouple position. Upon the arrival of the front wave, the temperature rapidly drops until the coldest wave passes through the runner. Subsequently, the temperature in the runner continues to rise, gradually approaching the set mold temperature. Consequently, after 30 seconds, the preheated pellets yield a higher runner temperature compared to the non-preheated pellets, measuring 1.63 °C for 2 pellets and 2.80 °C for 3 pellets.

Furthermore, a delayed arrival of the front wave is observed in the case of preheated pellets, despite using the same number of pellets. It is highly relevant to the initial melting status. The elastic modulus of the pellets drops rapidly from the glassy states to the rubbery states [12]. Preheating the pellets facilitates their transition into the rubbery state more rapidly, as it requires less heat transfer. In contrast, non-preheated pellets exhibit significant resistance to deformation upon reaching the melting surface due to their considerable elastic modulus. However, the top and side surfaces of these cold pellets can still melt and quickly fill the gaps in between due to gravitational forces.

Fig. 4(a) shows the density isosurface when the wave front reaches the runner exit ($t$=$t'$) and its evolution after 4 seconds ($t$=$t'$+4s). The light density region indicates the potential gas entrapment, as the pellets melt at both the bottom plunger surface and the top heat transfer plug surface. In this area, the flow converges, making it difficult for the trapped air to escape. After 4 seconds, a noticeable difference in density distribution remains in the previous flow convergence region, particularly in the area connecting to the runner. Thus, insufficient heat transfer in the case of non-preheated pellets can easily trap air in the flow convergence region, whereas preheated pellets can quickly deform and expel the trapped air.

To investigate the initial melting status, a short shot was executed by halting the plunger movement once the EMC flow reached the exit of the runner. The image of the remaining pellets is shown in Fig. 4(b). The pellet retains a dome shape because the top surface is positioned far from the heating element, while the side surface is in closer proximity to the hot sleeve sidewalls. Additionally, large voids are visible on the side surface, indicating that the gap-filling process has resulted in gas entrapment. Particularly in the side view in Fig. 4(b), the region connecting to the runner

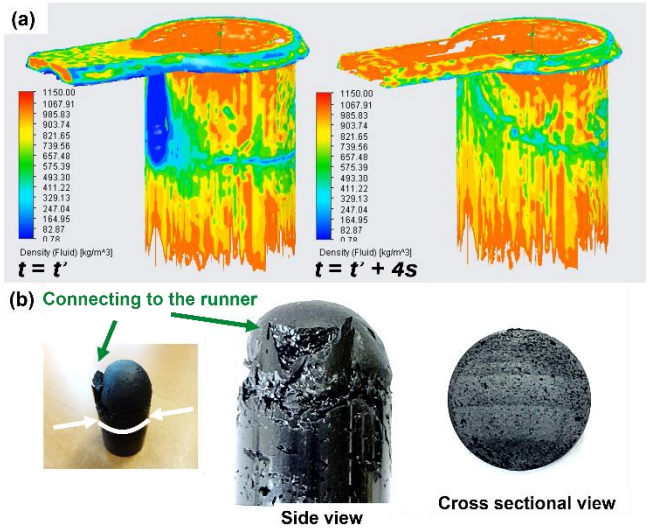


**Fig. 4** (a) Density isosurface (unit: kg/m$^3$) simulated when the flow reaches the runner exit and the status after 4 seconds. (b) Cross sectional view and side view of 3 non-preheated pellets after a short shot.

region remains more voids than the rest of the pellets, confirming the FEM simulation results.

Moreover, a cross-sectional view of the pellet was obtained through sawing as present in Fig. 4(b). This reveals a core region and a ring, distinguishable by their differing porosity. The core region originates from the original pellets, and the small voids present can be attributed to outgassing from the pellets' composition. In contrast, the ring region is characterized by larger voids, confirming its formation from the melted surface.

As a result, the delayed arrival of the front wave in the preheated pellets can be explained. Unlike the non-preheated pellets, the preheated pellets undergo simultaneous compression and melting. The deformed pellets effectively occupy the gaps, pushing gasses away. Theoretically, this reduces the entrapment of gas bubbles, leading to fewer voids in the molded product. Consequently, the front wave arrives later in the case of the preheated pellets.

Besides a delayed arrival of the front wave, in the case of preheated pellets, the wave with the lowest temperature arrives earlier before the transfer process completes. It indicates that a warmer EMC flow through the runner region after reaching the lowest temperature. However, the coldest wave of the non-preheated pellets arrives later than transfer being complete. It means temperature keeps dropping during the entire

transfer process. The temperature in the core of pellets at the final transfer stage was still low.

Figure 5 illustrates that the temperature drop time exhibits a linear relationship with the number of pellets. The temperature drop time in the runner region is defined as the duration from the arrival of the wave front to the point at which the lowest temperature is reached, as present in Fig. 3.

Specifically, adding one extra non-preheated pellet results in approximately 3.6 seconds of additional cold time in the runner region. In contrast, preheating significantly reduce the temperature drop time. Notably, the transfer of 3 preheated pellets results in a shorter temperature drop time even compared to 2 non-preheated pellets. Therefore, pellet preheating effectively prevents an extended cold period in the runner region.

Subsequently, the average temperature of the excessive EMC outside the runner was measured as shown in Fig. 5. The results indicate that 2 pellets yield a higher average temperature than 3 pellets under both preheating and non-preheating conditions. This observation is reasonable, as a larger number of pellets requires more thermal energy to raise the temperature.

However, preheated pellets exhibit a lower average temperature. The results indicate that, in this constant pressure-driven transfer process, preheated pellets complete the transfer process more quickly than non-preheated pellets. However, the average flow temperature of the preheated pellets remains lower than that of the non-preheated pellets for most of the duration.

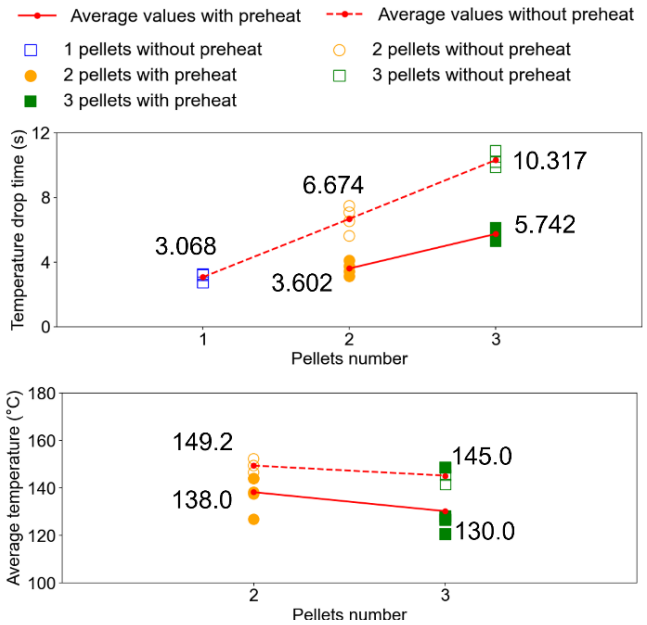


**Fig. 5** The average temperature of the excessive EMC and the average temperature drop time with different number of (non-)preheated pellets.

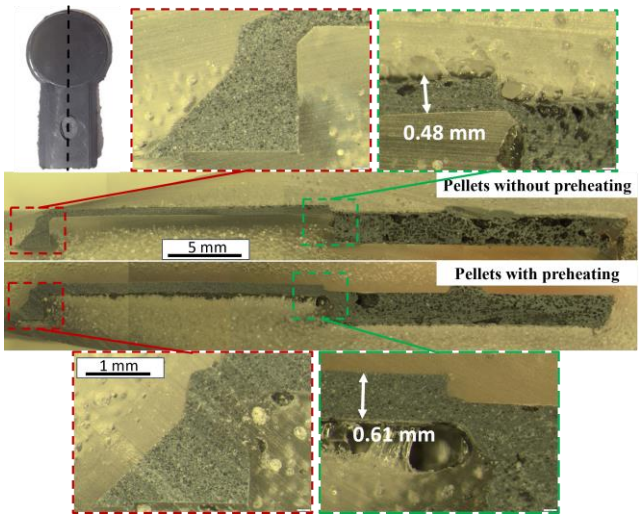


**Fig. 6** Cross-section of the culls formed by 3 (non-) preheated pellets. Right side is the runner exit.

This trend is consistent with the temperature evolution in Fig. 3. At the lowest point, the measured temperature for 3 preheated pellets is much lower than that of 3 non-preheated pellets, despite a similar plunger position. To investigate the underlying reasons, the cross sections of the culls formed by 3 pellets with and without preheating are examined, as shown in Fig. 6.

The cross-section can be divided into two parts. The left section is largely voidless because outgassing and trapped air bubbles are expelled by the plunger. A dense structure is achieved at the far end in both cases. However, a difference in thickness is observed under the same driving pressure. The non-preheated pellets resulted in a cull thickness of 0.48 mm cull while the preheated pellets produced a thicker cull measuring 0.61 mm. This difference can be attributed to the variation in flow temperature, as the process window narrows at higher temperatures with an increased reaction rate [13]. This observation is consistent with the results of the temperature evolution in Fig. 3, which indicate that after the 30 seconds test, the temperature of the preheated pellets is higher than that of the non-preheated pellets.

Furthermore, to understand the faster temperature dropping rate observed in the preheated pellets, additional differences can be noted in the right part of the cross-sections in Fig. 6, which represents the cured EMC in the runner region. In the case of non-preheated pellets, large voids are distributed along the top and bottom edges. These voids may form from trapped air in the gaps between the pellets and the sleeve, which is then carried into the runner area. In contrast, the central flow

ISBN: 978-3-8007-6541-6

contains smaller pores primarily resulting from outgassing. When pellets are preheated, porosity in the runner region is significantly reduced. Furthermore, a voidless gate region is achieved with the preheated pellets, while a few voids are present in the gate region of the non-preheated pellets.

### 3.3 Effect of preheating on the PLCC package

Figure 7 illustrates the process data, including the transfer pressure and the transfer velocity, during the transfer process. The transfer velocities closely align with the set values. In terms of transfer pressure evolution, the final period after the cavity is fully filled reflects a linear response from the plunger spring, which is consistent across different groups. However, a significant difference in transfer pressure is observed before the linear response period, attributed to the effects of preheating and transfer temperature.

After reaching the gate region, non-preheated pellets initially build up gate pressure earlier than preheated pellets. Subsequently, the pressure increases as the flow temperature steadily decreases, with the preheated pellets resulting in slightly higher pressure. This outcome corresponds to the recorded lower temperature associated with preheating as consistent with the measured average temperature. Furthermore, a molding temperature of 175 °C results in a lower transfer pressure in both preheated and non-preheated pellets. It is also associated to the higher flow temperature at a higher molding temperature.

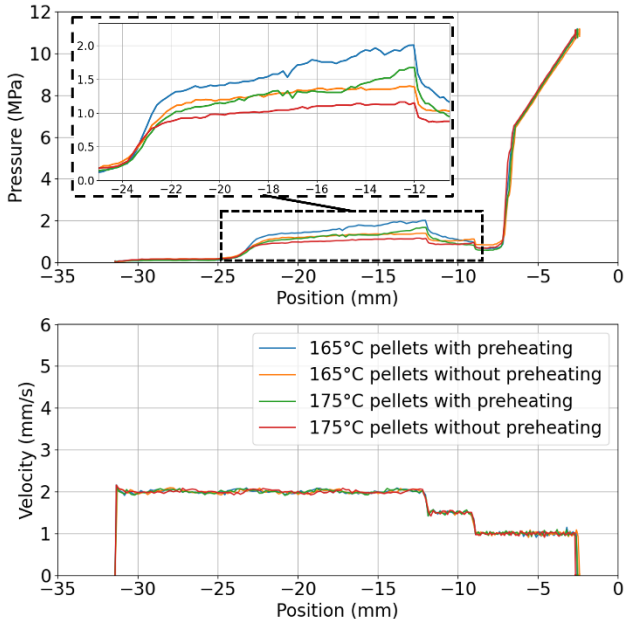


**Fig. 7** Process data of molding shots with (non-) preheated pellets at 165 °C and 175 °C.

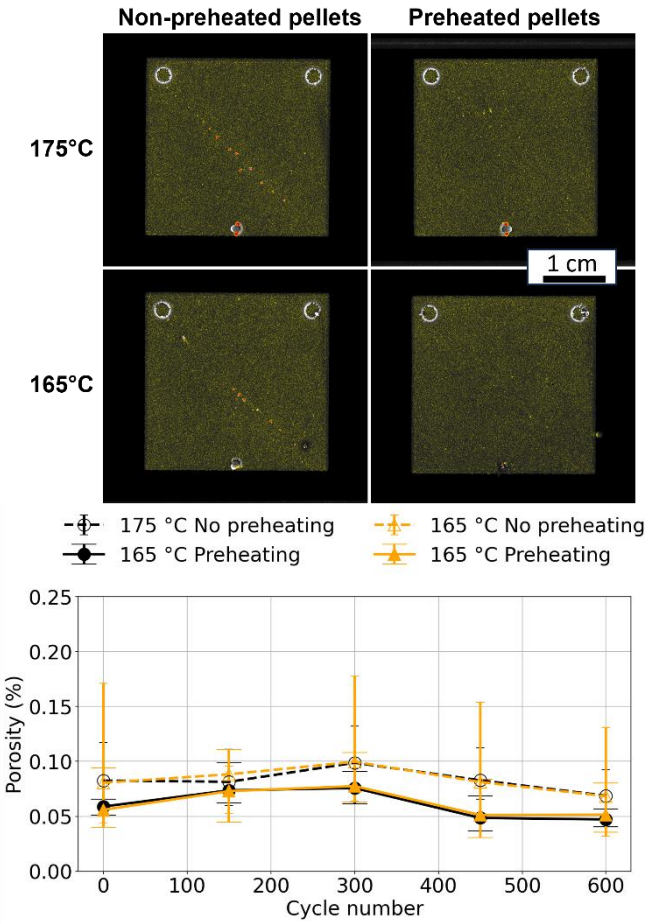


**Fig. 8** SAM images with void detection and the evolution of the porosity. Voids are marked as red.

The SAM results are shown in Fig. 8, with voids highlighted in red. It is important to note that the detected voiding in the ejection pin region should be disregarded due to the height difference on the surface.

3 non-preheated pellets generate more voids at 175 °C than at 165 °C because of more outgassing. However, preheating plays a more important role in reducing the voids compared to the molding temperature. Non-preheated pellets exhibit a distinct flow mark with considerable voids along it. According to the SAM, these voids are within the encapsulation instead of interfacial delamination. Thus, it can correlate to the results in the melting tests. Non-preheated pellets are more likely to entrap the air in the gaps between the sleeve and the pellets. In contrast, the voiding issue is significantly reduced with preheated pellets, although a diagonal flow mark remains slightly visible. At zero hour, the porosity for the non-preheated pellets at 175 °C and 165 °C are 0.083 % and 0.081 %, while the values for the preheated pellets are 0.059 % and 0.056 % at 175 °C and 165 °C, respectively.

ISBN: 978-3-8007-6541-6

The evolution of porosity in relation to the thermal aging number is plotted at the bottom of Fig. 8. All groups exhibit fluctuations without a clear trend. The results indicate a stable metal-polymer interface over a 600-hour HTS regardless of the molding temperature and pellet pretreatment.

Furthermore, the samples before and after 600 hours HTS test were inspected by optical microscope. A thermal oxide layer with brownish color is distinguishable in the specimens exposed for 600 hours, whereas it is not evident in the specimens at 0 hour.

As a result, the oxide layer in the specimen molded at 175 °C with non-preheated pellets exhibits the thickest oxide layer at 103.9±4.8 µm A similar oxide layer is observed in the specimen molded with non-preheated pellets at 165 °C, measuring 104.2±2.1 µm. In contrast, the specimen molded at 175 °C with preheated pellets shows the thinnest oxide layer at 88.8±5.8 µm.

The formation of the thermal oxide layer is attributed to two processes: the diffusion of oxygen and its reaction with the EMC [13]. In this study, since the aging temperature and the applied EMC are the same, a similar reaction rate of oxygen with EMC is expected, with oxygen diffusion primarily influencing the growth of the thermal oxide layer. Oxygen from the ambient environment diffuses into the EMC matrix through its porous network. Higher porosity can lead to a thicker thermal oxide layer, which aligns with the SAM results. This indicates that, compared to molding temperature, pellet preheating is an effective method for inhibiting thermal oxide growth by reducing porosity in the molded product.

## Conclusion

This research emphasizes the importance of pellet preheating in the EMC transfer molding process, and reliability enhancement, particularly for products that require encapsulation with a high mass of EMC.

In this study, the specific heat capacity of the EMC was first calibrated as 0.901 J/g·K. Subsequently, we investigated the effect of pellet preheating at 70 °C on melting performance and further encapsulation reliability in overmolded dummy PLCC leadframes using a research-oriented process recipe. The key findings of our research are as follows:

1. Preheating the pellets resulted in a denser EMC flow, which carried significantly less entrapped air. This improvement led to a notable reduction in the temperature drop time within the runner region of the molding process. However, it was observed that the gate pressure during the transfer molding process slightly increased.
2. The preheating of pellets proved to be more critical than the molding temperature in minimizing porosity within the package encapsulation. The reduction in porosity inhibited the growth of the thermal oxide layer during 600-hour HTS test, which is facilitated by the decreased diffusion paths for oxygen.

## Acknowledgement

This work was supported as part of the R-PODID project from the Chips Joint Undertaking and its members, including the top-up funding by National Authorities of Italy, Turkey, Portugal, The Netherlands, Czech Republic, Latvia, Greece, and Romania under grant agreement No. 101112338.


## References

[1] A. Ghannam, N. van Haare, J. Bravin, E. Brandl, B. Brandstätter, and H. Klingler: ‘Ultra-Thin QFN-Like 3D Package with 3D Integrated Passive Devices’, Proc. 2019 IEEE 69th Electronic Components and Technology Conference (ECTC), 2019

[2] S. H. M. Kersjes, J. L. J. Zijl, R. H. Poelma, and H. W. Wensink: ‘Transfer molding of primary LED optics; High aspect ratio domes’. Proc. 2013 Eurpoean Microelectronics Packaging Conference (EMPC), 2013

[3] N. Gaio, S. H. M. Kersjes, W. Q. Solano, P. Sarro, and R. Dekker: ‘Versatile and Automated 3D Polydimethylsiloxane (PDMS) Patterning for Large-Scale Fabrication of Organ-on-Chip (OOC) Components’. Proc. Eurosensors 2018, 2018

[4] Y. Yang, L. Dorn-Gomba, R. Rodriguez, C. Mak, and A. Emadi: ‘Automotive Power Module Packaging: Current Status and Future Trends’, IEEE Access, 2020, 8, pp. 160126-160144

[5] G. Q. Zhang, M. Graef, and F. Van Roosmalen: ‘The Rationale and Paradigm of "More than Moore"’. Proc. 2006 56th Electronic Components and Technology Conference, 2006

 

[6] K. F. Becker, D. Joklitschke, T. Braun, M. Koch, T. Thomas, T. Schreier-Alt, et al.: 'Transfer Molding Technology for Smart Power Electronics Modules: Materials and Processes', Journal of Microelectronics and Electronic Packaging, 2012, 9, (2), pp. 78-86

[7] A. J. Garete: 'Epoxy Molding Compound Development for Improved MSL1 Delamination Resistance in Plastic Encapsulated Clip Bond Power Package', Proc. 2020 IEEE 22nd Electronics Packaging Technology Conference (EPTC), 2020

[8] K. M. B. Jansen, J. d. Vreugd, L. J. Ernst, and C. Bohm: 'Thermal aging of molding compounds'. Proc. 2010 11th International Conference on Electronic Packaging Technology & High Density Packaging, Xi'an, China, 2011

[9] A. Inamdar, P. Gromala, A. Prisacaru, A. Kabakchiev, Y. Yang, and B. Han: 'EMC Oxidation Under High-Temperature Aging', pp. 53-80

[10] A. Keller, C. Dransfeld, and K. Masania: 'Flow and heat transfer during compression resin transfer moulding of highly reactive epoxies', Composites Part B: Engineering, 2018, 153, pp. 167-175

[11] JEDEC Solid State Technology Association: 'JESD22-A103D High Temperature Storage Life', 2010

[12] R. Li, D. Yang, P. Zhang, F. Niu, M. Cai, and G. Zhang: 'Effects of High-Temperature Storage on the Elasticity Modulus of an Epoxy Molding Compound', Materials, 2019, 12, (4), pp. 684

[13] C.-C. Su, C.-H. Wei, and B.-C. Li: 'Thermal and Cure Kinetics of Epoxy Molding Compounds Cured with Thermal Latency Accelerators', Advances in Materials Science and Engineering, 2013, (1), pp. 1-9

 